A Novel Fractal Way: Boolean Delay Equations, and Their Applications to the Geosciences

Michael Ghil [1] & Ilya Zaliapin [2]

This paper is the authors' contribution to the festivities honoring the 80th birthday of Benoît Mandelbrot. The "fractal sunburst" is our birthday gift.

Abstract. Boolean Delay Equations (BDEs) are a novel type of semi-discrete dynamical models with Boolean-valued variables that evolve in continuous time. Systems of BDEs can be classified into *conservative* or *dissipative*, in a manner that parallels the classification of ordinary or partial differential equations. Solutions to certain conservative BDEs exhibit growth of complexity in time. They represent therewith metaphors for biological evolution or human history.

Dissipative BDEs are structurally stable and exhibit multiple equilibria and limit cycles, as well as more complex, fractal solution sets, such as Devil's staircases and "fractal sunbursts." All the solutions of dissipative BDEs have stationary variance. BDE systems of this type, both free and forced, have been used as highly idealized models of climate change on interannual, interdecadal and paleoclimatic time scales.

BDEs are also being used as flexible, highly efficient models of colliding cascades in earthquake modeling and prediction, as well as in genetics. Some of the climatic and solid-earth applications will be briefly illustrated.

Keywords: Boolean Delay Equations, Complexity, Dynamical Systems, Earthquakes, El Niño/Southern Oscillation.

1 Introduction

BDEs are a novel modeling framework especially tailored for the mathematical formulation of conceptual models of systems that exhibit threshold behavior, multiple feedbacks and distinct time delays [10, 16, 17]. BDEs are intended as a heuristic first step on the way to understanding problems too complex to model using systems of partial differential equations at the present time. One hopes, of course, to be able to eventually write down and solve the exact equations that govern the most intricate phenomena. Still, in climate dynamics as well as in solid-earth geophysics and elsewhere in the natural sciences, much of the preliminary discourse is often conceptual.

[1]Département Terre-Atmosphère-Océan and Laboratoire de Météorologie Dynamique, Ecole Normale Supérieure, Paris, and Department of Atmospheric and Oceanic Sciences and Institute of Geophysics and Planetary Physics, University of California Los Angeles, USA. E-mail: ghil@lmd.ens.fr, corresponding author.

[2]Institute of Geophysics and Planetary Physics, University of California Los Angeles, USA. E-mail: zal@ess.ucla.edu

BDEs offer a formal mathematical language that may help bridge the gap between qualitative and quantitative reasoning. Besides, they are fun to play with and produce beautiful fractals [37, 38], by simple, purely deterministic rules.

In a hierarchical modeling framework, simple conceptual models are typically used to present hypotheses and capture isolated mechanisms, while more detailed models try to simulate the phenomena more realistically and test for the presence and effect of the suggested mechanisms by direct confrontation with observations [18]. BDE modeling may be the simplest representation of the relevant physical concepts. At the same time new results obtained with a BDE model often capture phenomena not yet found by using conventional tools [47, 59, 60]. These results suggest possible mechanisms that may be investigated using more complex models once their "blueprint" was seen in a simple conceptual model. As the study of complex systems garners increasing attention and is applied to diverse areas — from microbiology to the evolution of civilizations, passing through economics and physics — related Boolean and other discrete models are being explored more and more [8, 21, 29, 44, 57].

In this brief review, we first describe the general form and main properties of BDEs (Section 2). Next, we illustrate some applications, to climate dynamics (Section 3) and to earthquake physics (Section 4). The "fractal sunburst" appears in Fig. 3 of Section 3.5 and the highly intermittent, lacunary character of certain earthquake sequences is captured in Figs. 5 and 8 of Section 4. We conclude in Section 5 with some ways of enriching our knowledge of BDEs and of the fractals they produce.

2 Boolean Delay Equations (BDE)

BDEs may be classified as *semi-discrete dynamical systems*, where the variables are discrete — typically Boolean, *i.e.* taking the values 0 ("off") or 1 ("on") only — while time is allowed to be continuous. As such they occupy the previously "missing corner" in the rhomboid of Fig. 1, where dynamical systems are classified according to whether their time (t) and state variables (x) are continuous or discrete.

Systems in which both variables and time are continuous are called *flows* [3, 50] (upper corner in the rhomboid of Fig. 1). Vector fields, ordinary and partial differential equations (ODEs and PDEs), functional and delay-differential equations (FDEs and DDEs) and stochastic differential equations (SDEs) belong to this category. Systems with continuous variables and discrete time (middle left corner) are known as *maps* [7, 22] and include diffeomorphisms, as well as ordinary and partial difference equations (O$\triangle$Es and P$\triangle$Es). In automata (lower corner) both the time and the variables are discrete; cellular automata (CAs) and all Turing machines (including real-world computers) are part of this group [21, 57]. BDEs and their predecessors, kinetic [53] and conservative logic, complete the rhomboid in the figure and occupy the remaining middle right corner.

2.1 General form

Given a system with n continuous real-valued state variables $\vec{v} = (v_1, v_2, \ldots, v_n) \in \mathcal{R}^n$ for which natural thresholds $q_i \in \mathcal{R}$ exist, one can associate with each variable $v_i \in \mathcal{R}$ a Boolean-valued variable, $x_i \in \mathcal{B} = \{0, 1\}$, *i.e.*, a variable that is either "on" or "off," by letting

$$x_i = \begin{cases} 0, & v_i \leq q_i \\ 1, & v_i > q_i \end{cases}, \qquad i = 1, \ldots, n. \tag{1}$$

The equations that describe the evolution of the Boolean vector $\vec{x} = (x_1, x_2, \ldots, x_n) \in \mathcal{B}^n$ due to the time-delayed interactions between the Boolean variables $x_i \in \mathcal{B}$ are of the form:

$$\begin{cases} x_1 = f_1\left(x_1(t-\theta_{1,1}), x_2(t-\theta_{1,2}), \ldots, x_n(t-\theta_{1,n})\right), \\ x_2 = f_2\left(x_1(t-\theta_{2,1}), x_2(t-\theta_{2,2}), \ldots, x_n(t-\theta_{2,n})\right), \\ \qquad\qquad \vdots \\ x_n = f_n\left(x_1(t-\theta_{n,1}), x_2(t-\theta_{n,2}), \ldots, x_n(t-\theta_{n,n})\right). \end{cases} \tag{2}$$

The functions $f_i : \mathcal{B}^n \to \mathcal{B}$, $1 \leq i \leq n$, are defined via Boolean equations that involve logical operators and delays. Each delay value $\theta_{i,j} \in \mathcal{R}$, where $1 \leq i, j \leq n$, is the length of time it takes for a change in variable x_j to affect the variable x_i.

2.2 Some theoretical results

We summarize here a few basic theoretical results from BDE theory; their original and complete form appears in Ghil and Mullhaupt [16].

Existence and uniqueness of solutions. Consider a BDE system and piecewise-constant initial data over an interval equal in length to the longest delay. One can then prove by construction the existence of a unique solution by using a lemma that shows the absence of solutions with an infinite number of "jumps" (between 0 and 1) in any finite-time interval [10].

"Pigeon-hole" lemma. All BDE systems that possess only *rational* delays can be reduced in effect to finite cellular automata. Commensurability of the delays creates a partition of the time axis into segments over which state variables remain constant and whose length is an integer multiple of the delays' least common denominator. As there is only a finite number of possible assignments of two values to these segments, repetition must occur, and the only asymptotic behavior possible is eventual constancy or periodicity in time.

Classification. Ghil and Mullhaupt [16] classified BDE systems as follows: All systems with solutions that are immediately periodic for all rational delays are *conservative*, while systems that for some rational delays exhibit transient behavior before settling into eventual periodicity are *dissipative*. The differential dynamical systems analogs are conservative (*e.g.*, Hamiltonian) dynamical systems [20, 35] versus forced-dissipative systems (*e.g.*, the well-known Lorenz [36] system). Typical examples of conservative systems occur in celestial mechanics [2], while dissipative systems are often used in modeling geophysical phenomena [15].

Asymptotic behavior. The following types of asymptotic behavior were observed in BDE systems: *(a) Fixed point* — the solution reaches one of a finite number of possible states and remains there; *(b) limit cycle* — the solution becomes periodic after a finite time elapses; and *(c) growing complexity* — certain classes of BDEs with incommensurable delays were shown to have solutions with growing complexity, as measured by the number of jumps per unit time. This number grows like a positive, but fractional power of time t [10], with superimposed log-periodic oscillations [16].

Approximation theorem. The following theorem facilitates numerical exploration of solutions to BDE systems: All solutions to systems of BDEs can be approximated (with respect to an $\mathcal{L}_2$-norm) for a given finite time by the periodic solutions of a nearby system having rational delays only.

3 A BDE Model for El Niño/Southern Oscillation

The El-Niño/Southern-Oscillation (ENSO) phenomenon is the most prominent signal of seasonal-to-interannual climate variability. It was known for centuries to fishermen along the west coast of South America, who witnessed a seemingly sporadic and abrupt warming of the cold, nutrient-rich waters that caused havoc to their fish harvests [11, 45]. Its common occurrence shortly after Christmas inspired them to name it El Niño, after the "Christ child." Starting in the 1970s, El Niño's climatic effects were found to be far broader than just its off-shore manifestations [11, 19]. This realization led to a global awareness of ENSO's significance, and an impetus to attempt and improve predictions of exceptionally strong El Niño events [34].

3.1 Conceptual ingredients

Bjerknes [5], who laid the foundation of modern ENSO research, suggested a *positive feedback* as a mechanism for the growth of an internal instability that could produce large positive anomalies of sea surface temperatures (SSTs) in the eastern Tropical Pacific. Using observations from the International Geophysical Year (1957-58), he realized that this mechanism must involve *air-sea interaction* in the tropics.

Compensating for Bjerknes's positive feedback is a *negative feedback* in the system that allows a return to colder conditions in the basin's eastern part. This negative feedback involves the ocean's adjustment to the atmospheric forcing by means of planetary-scale waves that are trapped near the equator by the Coriolis force: faster Kelvin and slower Rossby waves that propagate across the ocean and ultimately cause a switch between the warm El Niño and cold La Niña phases of a seesaw in space and time. An important additional element is the seasonal forcing, which dictates the seasonal maxima of warming and cooling.

3.2 Model variables and equations

The model [47] operates with five Boolean variables. The state of the *ocean* is depicted by SST anomalies, expressed via a combination of two Boolean variables, T_1 and T_2. The relevant anomalous *atmospheric* conditions in the Equatorial Pacific basin are described by the variables U_1 and U_2. The latter express the state of the trade winds. For both the atmosphere and the ocean, the first variable, T_1 or U_1, describes the sign of the anomaly, positive or negative, while the second one, T_2 or U_2, describes its amplitude, strong or weak. Thus, each one of the pairs (T_1, T_2) and (U_1, U_2) defines a four-level discrete variable that represents highly positive, slightly positive, slightly negative, and highly negative deviations from the climatological mean. The *seasonal cycle's* external forcing is represented by a two-level Boolean variable S.

The atmospheric variables U_i are "slaved" to the ocean [41, 28]:

$$U_i(t) = T_i(t - \beta),\ i = 1, 2. \tag{3}$$

The evolution of the sign T_1 of the SST anomalies is modeled according to the Bjerknes hypothesis and involves oceanic wave adjustments:

$$T_1(t) = \{(R \wedge \neg U_1)(t - \tau)\} \vee \{\neg R(t - \tau) \wedge U_2(t - \beta)\}; \tag{4}$$

here the symbols $\vee$ and $\wedge$ represent the binary logical operators OR and AND, respectively. A Rossby-wave signal $R(t) = U_1(t) \triangle U_2(t)$ is defined via the binary Boolean operator $\triangle$ that takes on the value 1 if and only if both operands have the same value. The seasonal-cycle forcing S is given by $S(t) = S(t - 1)$; it affects the SST anomalies' amplitude T_2 through an enhancement of events when favorable seasonal conditions prevail:

$$T_2(t) = \{[S \triangle T_1](t - \beta)\} \vee \{[\neg(S \triangle T_1) \wedge T_2](t - \beta)\}. \tag{5}$$

The time t is thus measured in units of 1 year.

The model's principal parameters are two delays: β and τ; they are associated with local adjustment processes and with basin-wide processes, respectively. The changes in wind conditions are assumed to lag the SST variables by a short delay β, of the order of days to weeks. For the length of the delay τ we adopt Jin's [24] view of the delayed-oscillator mechanism and let it represent the time that elapses while combined processes

of oceanic adjustment occur: it may vary from about one month in the fast-wave limit [25, 26, 40] — to about two years.

3.3 Model solutions

Studying the ENSO phenomenon, we are primarily interested in the dynamics of the SST states, represented by the two-variable Boolean vector (T_1, T_2). To be more specific, we deal with a four-level scalar variable

$$ENSO = \begin{cases} -2, & \text{extreme La Niña}, & T_1 = 0, T_2 = 0, \\ -1, & \text{mild La Niña}, & T_1 = 0, T_2 = 1, \\ 1, & \text{mild El Niño}, & T_1 = 1, T_2 = 0, \\ 2, & \text{extreme El Niño}, & T_1 = 1, T_2 = 1. \end{cases} \tag{6}$$

Governed by the model equations, the $ENSO$ vector takes on values $\{-2, -1, 1, 2\}$, precisely in this order, thus simulating the real ENSO cycles. The cycles follow the same sequence of states, although the residence time within each state changes as τ changes. The period P of a simple oscillatory solution is defined as the time between the onset of two consecutive extreme warm events, $ENSO = 2$. We use the cycle period definition to classify different model solutions (see Fig. 2).

(i) Periodic solutions with a single cycle (simple period). Each succession of events, or *internal cycle*, is completely phase-locked here to the seasonal cycle, *i.e.*, the warm events always peak at the same time of year. For each fixed β, as τ is increased, intervals where the solution has a simple period equal to $2, 3, 4, 5, 6$, and 7 years arise consecutively.

(ii) Periodic solutions with several cycles (complex period). We describe such sequences, in which several distinct cycles make up the full period, by the parameter $\bar{P} = P/n$; where P is the length of the sequence and n is the number of cycles in the sequence. Notably, as we transition from a period of three years to a period of four years (see second inset of Fig. 2), $\bar{P}$ becomes a nondecreasing step function of τ that takes only rational values, arranged on a Devil's staircase.

3.4 The quasi-periodic (QP) route to chaos in the BDE model

The frequency-locking behavior observed for our BDE solutions above is a signature of the universal QP route to chaos. Its mathematical prototype is the Arnol'd circle map [3], given by the equation:

$$\theta_{n+1} = \theta_n + \Omega + 2\pi K \sin(2\pi\theta_n) \pmod 1. \tag{7}$$

Equation (7) describes the motion of a point denoted by the angle θ of its location on a unit circle that undergoes fixed shifts by an angle Ω along the circle's circumference. The point is also subject to nonlinear sinusoidal "corrections," with the size of the nonlinearity controlled by a parameter K.

We look at the winding number $\omega = \omega(\Omega, K) = \lim_{n\to\infty}[(\theta_n - \theta_0)/n]$, which can be described roughly as the average shift of the point per iteration. When the nonlinearity's influence is small, this average shift — and hence the average period — is determined largely by Ω; it may be rational or irrational, with the latter being more probable due to the irrationals' pervasiveness. As the nonlinearity K is increased, "Arnol'd tongues" — where the winding number ω locks to a constant rational over whole intervals — form and widen. At a critical parameter value, only rational winding numbers are left and a complete Devil's staircase crystallizes. Beyond this value, chaos reigns as the system jumps irregularly between resonances [23, 49].

The average cycle length $\bar{P}$ defined for our ENSO system of BDEs is clearly analogous to the circle map's winding number, in both its definition and behavior. Note that the QP route to chaos depends in an essential way on two parameters: Ω and K for the circle map and β and τ in our BDE model.

3.5 The "fractal sunburst": A "bizarre" attractor

As the system undergoes the transition from an averaged period of two to three years a much more complex, and heretofore unsuspected, "fractal sunburst" structure emerges (Fig. 3, and first inset in Fig. 2). As the wave delay τ is increased, mini-ladders build up, collapse or descend only to start climbing up again. In the vicinity of a critical value ($\tau \cong 0.5$ years), the pattern's focal point, these mini-ladders rapidly condense and the structure becomes self-similar, as each zoom reveals the pattern being repeated on a smaller scale. We call this a "bizarre attractor" because it is more than "strange": the latter attractors occur in a system's parameter space, for fixed parameter values, the former is a structure that appears in our model's phase-parameter space, like the Devil's staircase.

The influence of the local-process delay β, along with that of the wave-dynamics delay τ, is shown in the three-dimensional "Devil's bleachers" (or "Devil's terrace," according to Jin *et al.* [28]) of Fig. 4. Note that the Jin *et al.* [27, 28] model is an intermediate model, in the terminology of modeling hierarchies [18]: it is based on a system of nonlinear PDEs in one space dimension (longitude along the equator). The Devil's bleachers in our BDE model resemble fairly well those in the intermediate ENSO model of Jin *et al.* [28]. The latter, though, did not exhibit a "fractal sunburst," which appears, on the whole, to be an entirely new addition to the fractal picture gallery [37, 38].

4 A BDE Model for Seismicity

Lattice models of systems of interacting elements are widely applied for modeling seismicity, starting from the pioneering works of Burrige and Knopoff [6], Allègre *et al.* [1], and Bak *et al.* [4]. The state of the art is summarized in [31, 32, 42, 46, 55]. Recently, colliding cascade models [12, 13, 59, 60] have been able to reproduce a wide set of observed characteristics of earthquake dynamics [30, 48, 54]: (i) the seismic cycle;

(ii) intermittency in the seismic regime; (iii) the size distribution of earthquakes, known as the Gutenberg-Richter relation; (iv) clustering of earthquakes in space and time; (v) long-range correlations in earthquake occurrence; and (vi) a variety of seismicity patterns premonitory to a strong earthquake. Some of this progress is due to using BDEs for modeling the colliding cascade phenomena.

4.1 Conceptual ingredients

Colliding cascade models [12, 13, 59, 60] synthesize three phenomena that play an important role in many complex systems: (i) the system has a hierarchical structure; (ii) the system is continuously loaded (or driven) by external sources; and (iii) the elements of the system fail (break down) under the load, causing redistribution of the load and strength throughout the system. Eventually the failed elements heal, thereby ensuring the continuous operation of the system.

The load is applied at the top of the hierarchy and transferred downwards, thus forming a *direct cascade of loading*. Failures are initiated at the lowest level of the hierarchy, and gradually propagate upwards, thereby forming an *inverse cascade of failures*, which is followed by healing. The interaction of direct and inverse cascades establishes the dynamics of the system: loading triggers the failures, and failures redistribute and release the load. In its applications to seismicity, the model's hierarchical structure represents a fault network, loading imitates the effect of tectonic forces, and failures imitate earthquakes.

4.2 Model structure and parameters

Our BDE model [59, 60] acts on a ternary tree, where each element is connected to and interacts with its six nearest neighbors: the parent, two siblings, and three children. At each epoch a given element may be either *intact* or *failed (broken)*, and either *loaded* or *unloaded*. The state of an element e at a moment n is thus defined by two Boolean functions $s_e(n) =$‘intact’ or ‘failed’} and $l_e(n) =$‘unloaded’ or ‘loaded’}. An element of the system may switch from one state to another under an impact from its nearest neighbors and external sources.

The dynamics of the system is controlled by the time delays between the given impact and switching to another state. The two primary delays are the loading time Δ_L necessary for an unloaded element to become loaded under the impact of its parent, and the healing time Δ_H necessary for a broken element to recover. Failures are initiated randomly within the elements at the lowest level.

4.3 Model solutions

The output of the model is a catalog of earthquakes — *i.e.,* of failures of its elements — similar to the simplest routine catalogs of observed earthquakes:

$$\mathcal{C} = (t_k,\ m_k,\ h_k),\ k = 1, 2, \ldots;\ t_k \leq t_{k+1}. \tag{8}$$

Here t_k is the starting time of the rupture; m_k is the magnitude, a logarithmic measure of energy released by the earthquake; and h_k is the vector that comprises the coordinates of the hypocenter. The latter is a point approximation of the area where the rupture started.

The quantitative description of model earthquake sequences is given by two measures. The first is the density $\rho(n)$ of the elements that are in a failed state at the moment n:

$$\rho(n) = \left[\nu_1(n) + \ldots + \nu_m(n)\right]/m. \tag{9}$$

Here $\nu_i(n)$ is the fraction of failed elements at the i-th level of the hierarchy at the moment n, while m is the depth of the tree. In this review, we will only consider this measure averaged over a time interval I and will denote it by $\rho(I)$.

The second measure is the irregularity $G(I)$ of energy release over the time interval I; its complete technical definition is somewhat complicated to be reproduced here; see [59]. Nonetheless, G has a transparent intuitive interpretation: it equals unity for a catalog consisting of a single event (delta function, burst of energy), and it is zero for a marked Poisson process (uniform energy release). Generally, it takes values between 0 and 1 depending on the irregularity of the observed energy release.

4.4 Seismic regimes

The model produces synthetic sequences that can be divided into three seismic regimes, illustrated in Fig. 5. Regime **H** corresponds to *high and nearly periodic seismicity* (top panel). The fractures within each cycle always reach the top level. The sequence is approximately periodic, in the statistical sense of cyclo-stationarity. Regime **I** exhibits *intermittent seismicity* (middle panel). The seismicity reaches the top level for some but not all cycles. Regime **L** is characterized by *medium or low seismicity* (lower panel). No cycle reaches the top level and seismic activity is much more constant at a low or medium level, without the long quiescent intervals present in Regimes **H** and **I**. The location of these three regimes in the plane of the two key parameters (Δ_L, Δ_H) is shown in Fig. 6.

4.5 Bifurcation diagram

Figure 7 illustrates the transition between regimes in the parameter plane (Δ_L, Δ_H). Panel (a) shows a rectangular trajectory in this plane that passes through all three regimes and touches the triple point. We single out 30 points along this trajectory; they are indicated by small circles in the figure. The three pairs of points that correspond to

the transitions between regimes are distinguished by larger circles and marked in addition by letters, for example (A) and (B) mark the transition from Regime **H** to Regime **L**.

We estimate the clustering $G(I)$ and average density $\rho(I)$ over the time interval $I = [0,\ 2 \cdot 10^6]$, for representative synthetic sequences that correspond to the 30 marked points along the rectangular path in Fig. 7a; they are shown in Fig. 7b. The values of G drop dramatically, from 0.8 to 0.18, between points (A) and (B): this means that the energy release switches from highly irregular to almost uniform between Regimes **H** and **L**. This transition, however, barely changes the average density ρ of failures.

The transitions between the other pairs of regimes are much smoother. The clustering drops further, from $G = 0.18$ to $G \approx 0.1$, and then remains at the latter low level within Regime **L**. It increases gradually, albeit not monotonically, from 0.1 to 0.8 between points (C) and (A), on its way through regimes **I** and **H**. The increase of Δ_L along the right side of the rectangular trajectory corresponds to a fixed level of clustering, $G \approx 0.8$.

The transition between regimes is illustrated further in Fig. 8. Each panel shows a fragment of the six synthetic sequences that correspond to the points (A)–(F) in Fig. 7a. The sharp difference in the character of the energy release at the transition between Regimes **H** (point (A)) and **L** (point (B)) is very clear, here too. The other two transitions, from (C) to (D) and (E) to (F), are much smoother. Still, they highlight the intermittent character of Regime **I**, to which points (D) and (E) belong.

5 What Next?

While the development and applications of BDEs started about two decades ago, this is a very short time span compared to ODEs, PDEs, maps, and even cellular automata. The results obtained so far, though, are sufficiently intriguing to warrant further exploration.

Methodologically, one might wish to explore "partial BDEs" in which the number of Boolean variables is quite large or even infinite. These systems stand in the same relation to "ordinary BDEs," explored so far, as PDEs do to ODEs. One can easily imagine some basic results for hyperbolic partial BDEs, where all the operators that connect spatially adjacent variables are conservative, as well as for parabolic ones, where the operators would include also some dissipative ones. Wright *et al.* [58] have already considered ensemble averaging over BDE solutions with randomized initial data. It would be even more interesting to consider the random perturbation of delays.

From the point of view of applications, BDEs have been applied fairly extensively by now to climate dynamics [17, 33, 39, 43, 58] and are making significant inroads into solid-earth geophysics [59, 60]. Most interesting is the recent application to the life sciences (Oktem *et al.* [44]), which represents in a sense a return to the concepts of the geneticist René Thomas, originator of kinetic logic [51, 52, 53].

It would appear that BDEs are well suited for the exploration of poorly understood phenomena in the socio-economic realm. Moreover, the robustness of fairly regular solutions in a wide class of BDEs, for many sets of delays and a variety of initial states, suggests interesting applications to certain issues in massively parallel computations.

Acknowledgements. It is a pleasure to thank the Académie Européenne Interdisciplinaire des Sciences and the organizers of the International Conference honoring Benoît Mandelbrot's 80th birthday for the invitation to deliver a talk on this joyous occasion. We are indebted to all the collaborators who helped us formulate, analyze and apply BDEs: *D. Dee* (NASA Goddard), *V. I. Keilis-Borok* (IGPP, UCLA & MITPAN, Moscow), *A. P. Mullhaupt* (Wall Street), *P. Pestiaux* (Total, France), and *A. Saunders* (Magnet High School, Van Nuys). This work was supported by NSF Grant ATM-0082131 and by the European Commission's NEST project "Extreme Events: Causes and Consequences (E2-C2)."

References

[1] Allègre, C. J., J. L. Le Mouel, and A. Provost, 1982. Scaling rules in rock fracture and possible implications for earthquake prediction. *Nature*, 297, 47-49.

[2] Arnol'd, V. I., 1978. *Mathematical Methods of Classical Mechanics*, Springer-Verlag, New York, 462 pp.

[3] Arnol'd, V. I., 1983. *Geometrical Methods in the Theory of Ordinary Differential Equations.* Springer-Verlag, New York.

[4] Bak, P., C. Tang, and K. Wiesenfeld, 1988. Self-organized criticality. *Phys. Rev. A*, 38, 364-374.

[5] Bjerknes, J., 1969, Atmospheric teleconnections from the equatorial Pacific. *Mon. Wea. Rev.*, 97, 163-172.

[6] Burridge, R., and L. Knopoff, 1967. Model and theoretical seismicity, *Bull. Seism. Soc. Am.*, 57, 341-371.

[7] Collet, P., and J.-P. Eckmann, 1980. *Iterated Maps on the Interval as Dynamical Systems.* Birkhäuser Verlag, Basel/Boston/Birkhäuser.

[8] Cowan, G. A., D. Pines and D. Melzer, Eds., 1994. *Complexity: Metaphors, Models and Reality.* Addison-Wesley, Reading, Mass.

[9] Darby, M. S., and L. A. Mysak, 1993. A Boolean delay equation model of an interdecadal Arctic climate cycle. *Climate Dyn.*, 8, 241-246.

[10] Dee, D., and M. Ghil, 1984. Boolean difference equations, I: Formulation and dynamic behavior. *SIAM J. Appl. Math.*, 44, 111-126.

[11] Diaz, H. F., and V. Markgraf, Eds., 1992. *El Niño: Historical and Paleoclimatic Aspects of the Southern Oscillation.* Cambridge Univ Press, New York.

[12] Gabrielov, A., V. Keilis-Borok, I. Zaliapin, and W. I. Newman, 2000a. Critical transitions in colliding cascades, *Phys. Rev. E*, 62, 237-249.

[13] Gabrielov, A.M., I. V. Zaliapin, V. I. Keilis-Borok, and W. I. Newman, 2000b. Colliding cascades model for earthquake prediction. *J. Geophys. Intl.*, 143, 427-437.

[14] Ghil, M., 1994. Cryothermodynamics: The chaotic dynamics of paleoclimate, *Physica D*, 77, 130-159.

[15] Ghil, M., and S. Childress, 1987. *Topics in Geophysical Fluid Dynamics: Atmospheric Dynamics, Dynamo Theory and Climate Dynamics*, Springer-Verlag, New York/Berlin/London/Paris/ Tokyo, 485 pp.

[16] Ghil, M., and A. P. Mullhaupt, 1985. Boolean delay equations. II: Periodic and aperiodic solutions. *J. Stat. Phys.*, 41, 125-173.

[17] Ghil, M., A. P. Mullhaupt, and P. Pestiaux, 1987. Deep water formation and Quaternary glaciations. *Clim. Dyn.*, 2, 1-10.

[18] Ghil, M., and A. W. Robertson, 2000. Solving problems with GCMs: General circulation models and their role in the climate modeling hierarchy. in D. Randall (Ed.) *General Circulation Model Development: Past, Present and Future*, Academic Press, San Diego, pp. 285-325.

[19] Glantz, M. H., R. W. Katz, and N. Nicholls, Eds. 1991. *Teleconnections Linking Worldwide Climate Anomalies.* New York: Cambridge Univ. Press.

[20] Guckenheimer, J., and P. Holmes, 1997. *Nonlinear Oscillations, Dynamical Systems and Bifurcations of Vector Fields.* 3rd edn., Springer-Verlag, New York.

[21] Gutowitz, H., 1991. *Cellular Automata: Theory and Experiment.* MIT Press, Cambridge, MA.

[22] Hénon, M., 1966. La topologie des lignes de courant dans un cas particulier. *C. R. Acad. Sci. Paris.*, 262, 312-414.

[23] Jensen, M. H., P. Bak, and T. Bohr, 1984. Transition to chaos by interaction of resonances in dissipative systems. Part I. Circle maps. *Phys. Rev. A*, 30, 1960-1969.

[24] Jin, F.-f., 1996. Tropical ocean-atmosphere interaction, the Pacific cold tongue, and the El-Niño-Southern Oscillation. *Science*, 274, 76-78.

[25] Jin F.-f., and J. D. Neelin, 1993a. Modes of interannual tropical ocean–atmosphere interaction — a unified view. I. Numerical results. *J. Atmos. Sci.*, 50, 3477-3503.

[26] Jin, F.-f., and J. D. Neelin, 1993b. Modes of interannual tropical ocean–atmosphere interaction — a unified view. III. Analytical results in fully coupled cases. *J. Atmos. Sci.*, 50, 3523-3540.

[27] Jin, F.-f., J. D. Neelin, and M. Ghil, 1994. El Niño on the Devil's Staircase: Annual subharmonic steps to chaos, *Science*, 264, 70-72.

[28] Jin, F.-f., J. D. Neelin, and M. Ghil, 1996. El Niño/Southern Oscillation and the annual cycle: Subharmonic frequency locking and aperiodicity, *Physica D*, 98, 442-465.

[29] Kauffman, S. A., 1995. *At Home in the Universe: The Search for Laws of Self-Organization and Complexity.* Oxford University Press, New York.

[30] Keilis-Borok, V. I., 1996. Intermediate-term earthquake prediction. *Proc. Natl. Acad. Sci. USA*, 93, 3748-3755.

[31] Keilis-Borok, V. I., 2002. Earthquake prediction: State-of-the-art and emerging possibilities. *Annu. Rev. Earth Planet. Sci.*, 30, 1-33.

[32] Keilis-Borok, V. I. and Shebalin, P. N., Eds., 1999. Dynamics of lithosphere and earthquake prediction. *Phys. Earth Planet. Int.*, 111, 179-330.

[33] Kellogg, W. W., 1983. Feedback mechanisms in the climate system affecting future levels of carbon dioxide. *J. Geophys. Res.*, 88, 1263-1269.

[34] Latif, M., T. P. Barnett, M. Flügel, N. E. Graham, J.-S. Xu, and S. E. Zebiak, 1994. A review of ENSO prediction studies. *Clim. Dyn.*, 9, 167-179.

[35] Lichtenberg, A. J., and M. A. Liebermann, 1992. 2nd edn., *Regular and Chaotic Motion*, Springer-Verlag, New York.

[36] Lorenz, E. N., 1963. Deterministic nonperiodic flow. *J. Atmos. Sci.*, 20, 130-141.

[37] Mandelbrot, B., 1975. *Les Objets Fractals: Forme, Hasard et Dimension.* Flammarion, Paris, 192 pp.

[38] Mandelbrot, B., 1982. *The Fractal Geometry of Nature.* W. H. Freeman & Co., New York, xii + 461 + xvi pp.

[39] Mysak, L. A., D. K. Manak, and R. F. Marsden, 1990. Sea-ice anomalies observed in the Greenland and Labrador Seas during 1901-1984 and their relation to an interdecadal Arctic climate cycle. *Climate Dyn.*, 5, 111-113.

[40] Neelin, J. D., and F.-f. Jin, 1993. Modes of interannual tropical ocean–atmosphere interaction — a unified view. II. Analytical results in fully coupled cases. *J. Atmos. Sci.*, 50, 3504-3522.

[41] Neelin, J. D., M. Latif, and F.-f. Jin, 1994. Dynamics of coupled ocean-atmosphere models: the tropical problem. *Annu. Rev. Fluid Mech.*, 26, 617-659.

[42] Newman, W. I., A. M. Gabrielov, and D. L. Turcotte, Eds., 1994. *Nonlinear Dynamics and Predictability of Geophysical Phenomena*, Geophys. Monographs Ser. 83, American Geophysical Union, Washington, DC.

[43] Nicolis, C., 1982. Boolean approach to climate dynamics. *Q. J. R. Meteorol. Soc.*, 108, 707-715.

[44] Oktem, H., R. Pearson, and K. Egiazarian, 2003. An adjustable aperiodic model class of genomic interactions using continuous time Boolean networks (Boolean delay equations). *Chaos*, 13, 1167-1174.

[45] Philander, S. G. H., 1990. *El Niño, La Niña, and the Southern Oscillation*, Academic Press, San Diego.

[46] Rundle, J. B., D. L. Turcotte, and W. Klein, Eds., 2000. *Geocomplexity and the Physics of Earthquakes*. American Geophysical Union, Washington, DC.

[47] Saunders, A., and M. Ghil, 2001. A Boolean delay equation model of ENSO variability. *Physica D*, 160, 54-78.

[48] Scholz, C. H., 1990. *The Mechanics of Earthquakes and Faulting.* Cambridge University Press, Cambridge.

[49] Schuster, H. G., 1988. *Deterministic Chaos: An Introduction.* Physik-Verlag, Weinheim.

[50] Smale, S., 1967. Differentiable dynamical systems. *Bull. Amer. Math. Soc.*, 73, 747-817.

[51] Thomas, R., 1973. Boolean formalization of genetic control circuits. *J. Theoret. Biol.*, 42, 563-585.

[52] Thomas, R., 1978. Logical analysis of systems comprising feedback loops. *J. Theoret. Biol.*, 73, 631-656.

[53] Thomas, R., Ed., 1979. *Kinetic Logic: A Boolean Approach to the Analysis of Complex Regulatory Systems*, Springer-Verlag, Berlin/Heidelberg/New York, 507 pp.

[54] Turcotte, D. L., 1997. *Fractals and Chaos in Geology and Geophysics*, 2nd edn., Cambridge University Press, Cambridge.

[55] Turcotte, D. L., W. I. Newman, and A. M. Gabrielov, 2000. A statistical physics approach to earthquakes. In: J. B. Rundle, D. L. Turcotte, and W. Klein, Eds., *Geocomplexity and the Physics of Earthquakes*. American Geophysical Union, Washington, DC, pp. 83-96.

[56] Tziperman, E., L. Stone, M. Cane, and H. Jarosh, 1994. El Niño chaos: Overlapping of resonances between the seasonal cycle and the Pacific ocean-atmosphere oscillator. *Science*, 264, 72-74.

[57] Wolfram, S., 1994. *Cellular Automata and Complexity: Collected Papers.* Addison-Wesley, Reading, Mass.

[58] Wright, D. G., T. F. Stocker, and L. A. Mysak, 1990. A note on Quaternary climate modeling using Boolean delay equations. *Clim. Dyn.*, 4, 263-267.

[59] Zaliapin, I., V. Keilis-Borok, and M. Ghil, 2003a. A Boolean delay equation model of colliding cascades. Part I: Multiple seismic regimes. *J. Stat. Phys.*, 111, 815-837.

[60] Zaliapin, I., V. Keilis-Borok, and M. Ghil, 2003b. A Boolean delay equation model of colliding cascades. Part II: Prediction of critical transitions. *J. Stat. Phys.*, 111, 839-861.

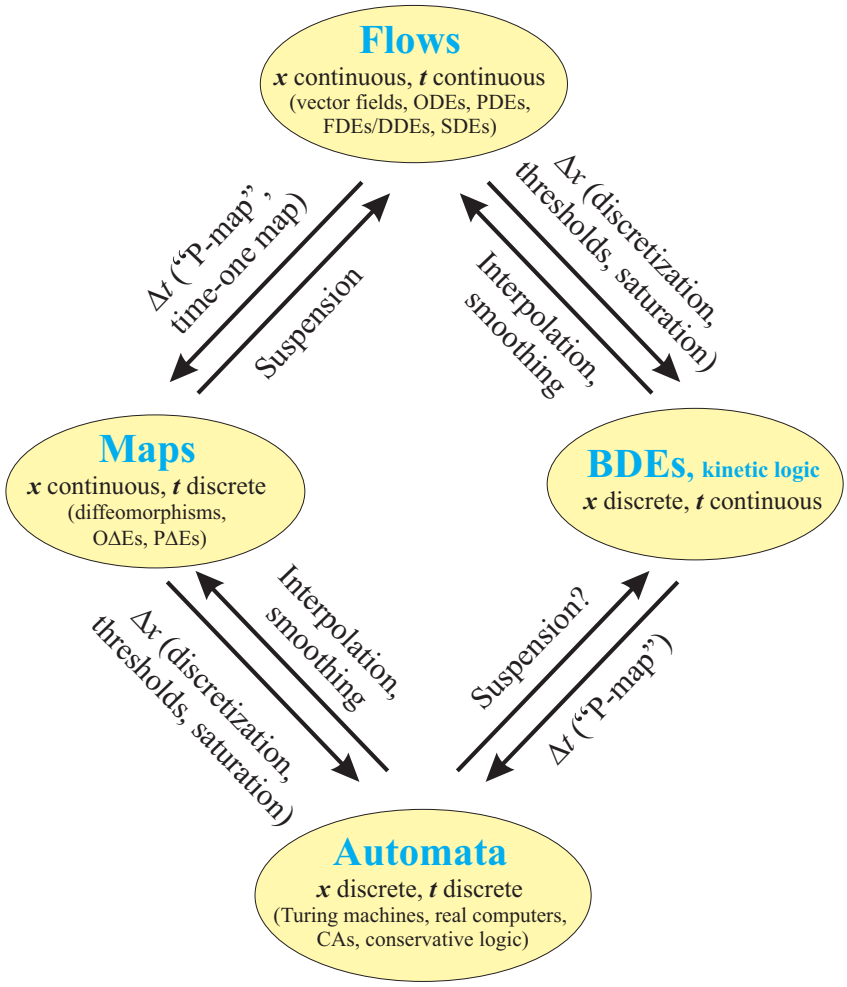

Figure 1: The place of BDEs within dynamical system theory. Note the links: The discretization of t can be achieved by the Poincaré map (P-map) or a time-one map, leading from **Flows** to **Maps**. The opposite connection is achieved by suspension. To go from **Maps** to **Automata** we use the discretization of x. Interpolation and smoothing can lead in the opposite direction. Similar connections lead from **BDEs** to **Automata** and to **Flows**, respectively.

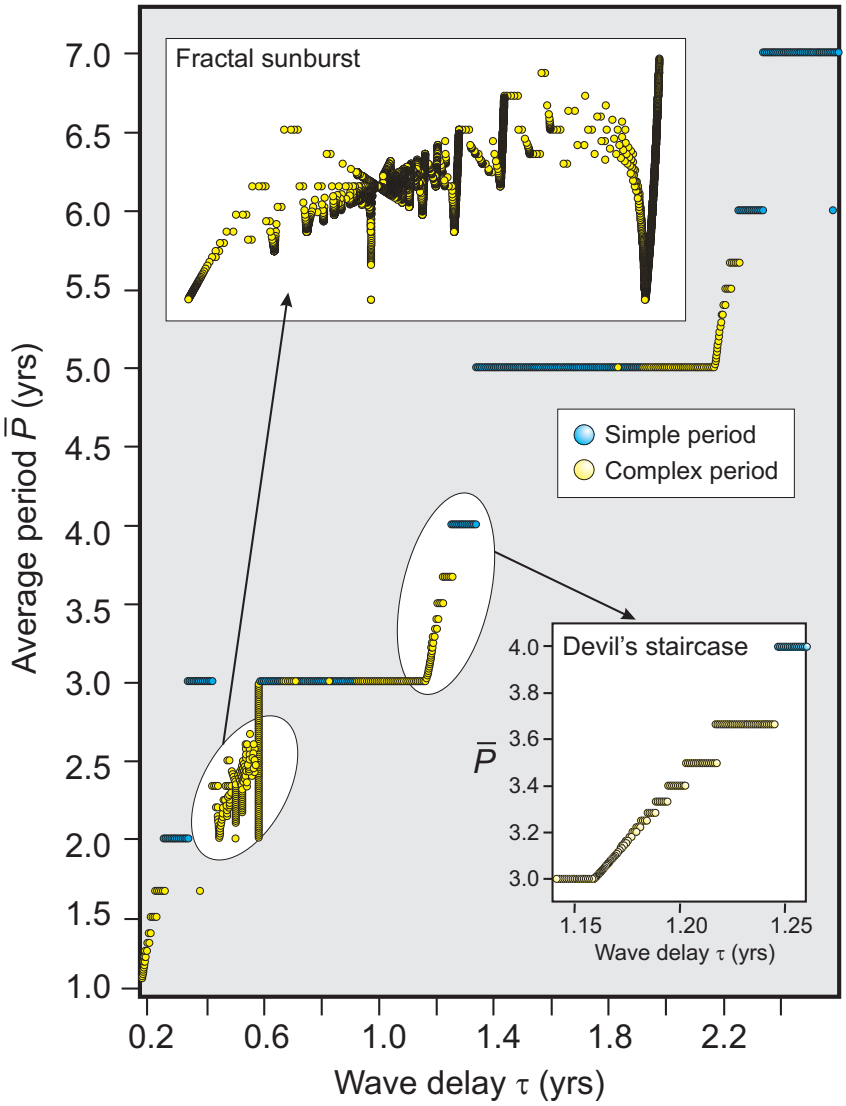

Figure 2: Devil's staircase and fractal sunburst: A bifurcation diagram showing the average cycle length $\bar{P}$ vs. the wave delay τ for a fixed $\beta = 0.17$. Blue dots indicate purely periodic solutions; orange dots are for complex periodic solutions; small black dots denote aperiodic solutions. The two insets show a blow-up of the overall, approximate Devil's staircase between periodicities of two and three years ("fractal sunburst") and of three and four years ("Devil's staircase").

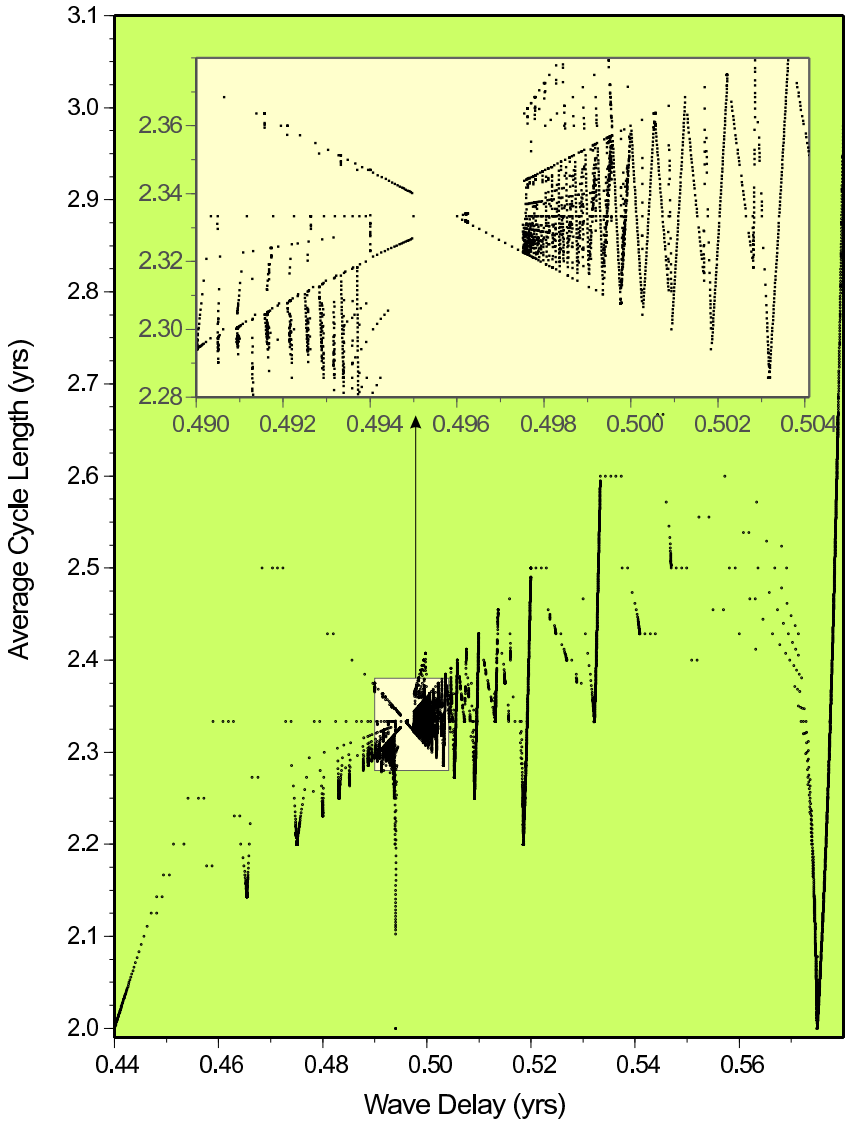

Figure 3: Fractal sunburst: a BDE solution pattern in phase-parameter space. A blow-up of the transition zone from average periodicity two to three years; $\tau = 0.4$–$0.58, \beta = 0.17$. The inset is a zoom on $0.49 \leq \tau \leq 0.504$. A complex mini-staircase structure reveals self-similar features, with a focal point at $\tau \approx 0.5$.

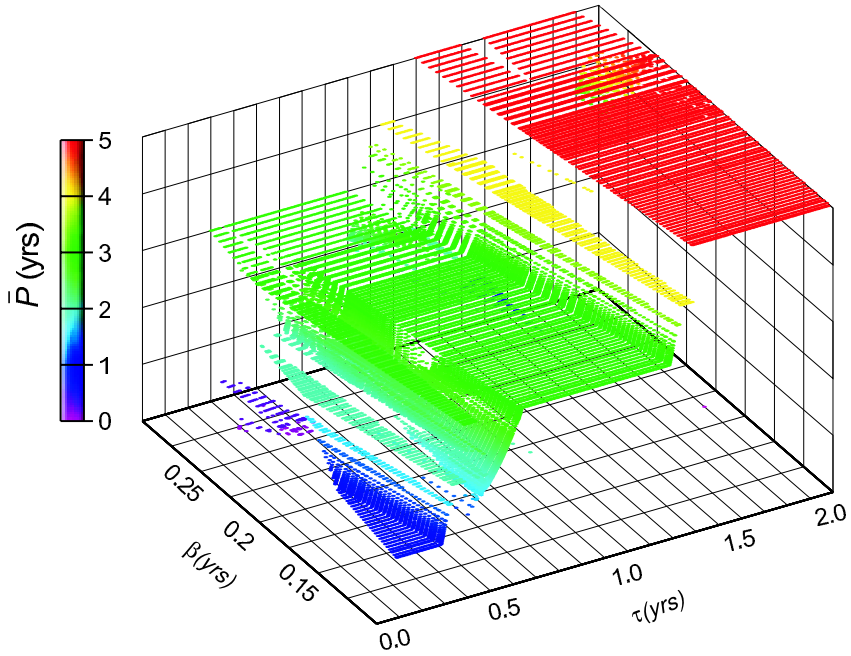

Figure 4: The Devil's bleachers: A three-dimensional regime diagram showing the average cycle length $\bar{P}$, portrayed in both height and color, vs. the two delays β and τ. Oscillations are produced even for very small values of β, as long as $\beta \leq \tau$. Variations in τ determine the oscillation's period, while changing β establishes the bottom step of the staircase, shifts the location of the steps, and determines their width.

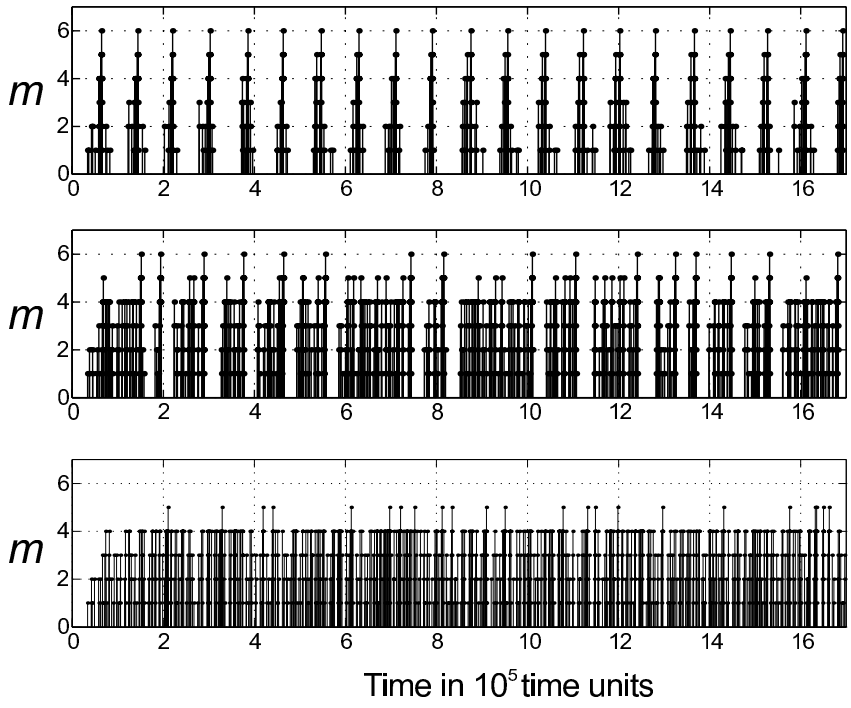

Figure 5: Three seismic regimes: sample of earthquake sequences. Top panel – regime **H** (High), $\Delta_H = 0.5 \cdot 10^4$; middle panel – regime **I** (Intermittent), $\Delta_H = 10^3$; bottom panel – regime **L** (Low), $\Delta_H = 0.5 \cdot 10^3$. Only a small fraction of each sequence is shown, to illustrate the differences between regimes.

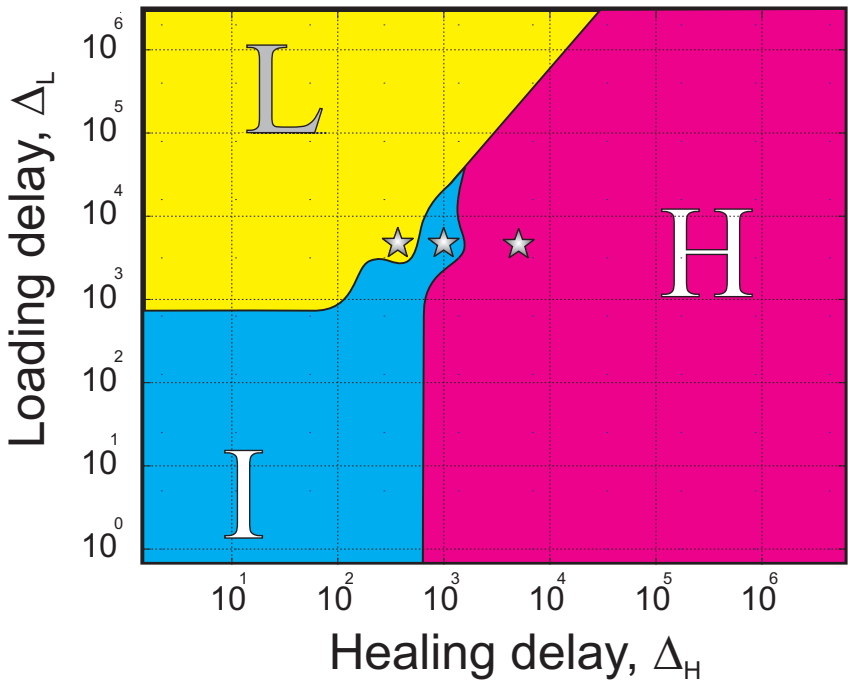

Figure 6: Regime diagram in the (Δ_L, Δ_H) plane of the loading and healing delays. Stars correspond to the sequences shown in Fig. 5.

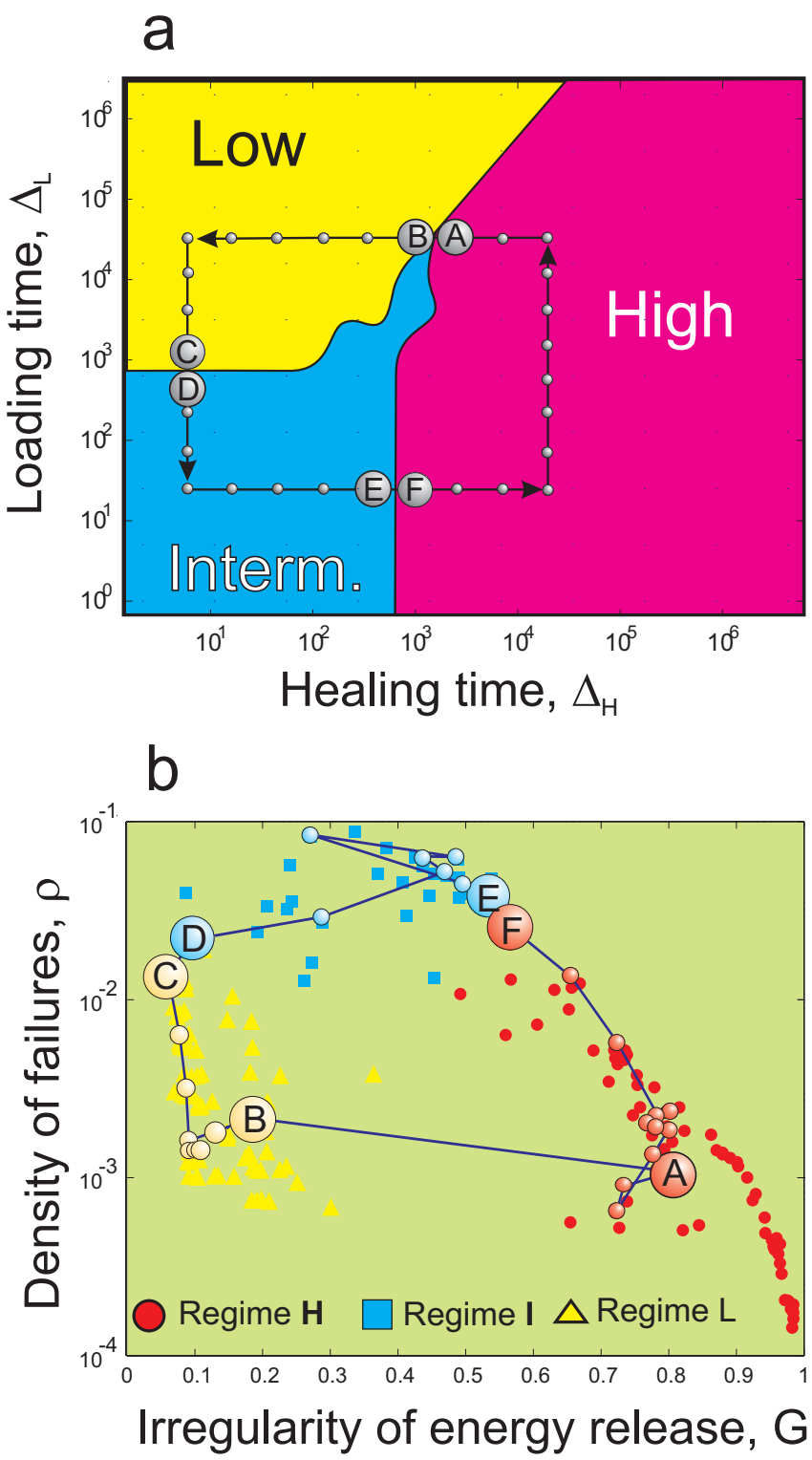

Figure 7: Bifurcation diagram for the BDE seismic model. a) Closed trajectory in the delay plane (Δ_L, Δ_H); b) The measures G and ρ, calculated along the parameter-plane trajectory shown in panel (a). The transition between points (A) and (B), *i.e.* between regimes **H** and **L**, is very sharp according to the irregularity of energy release (G). At the same time, it is almost negligible by the measure ρ.

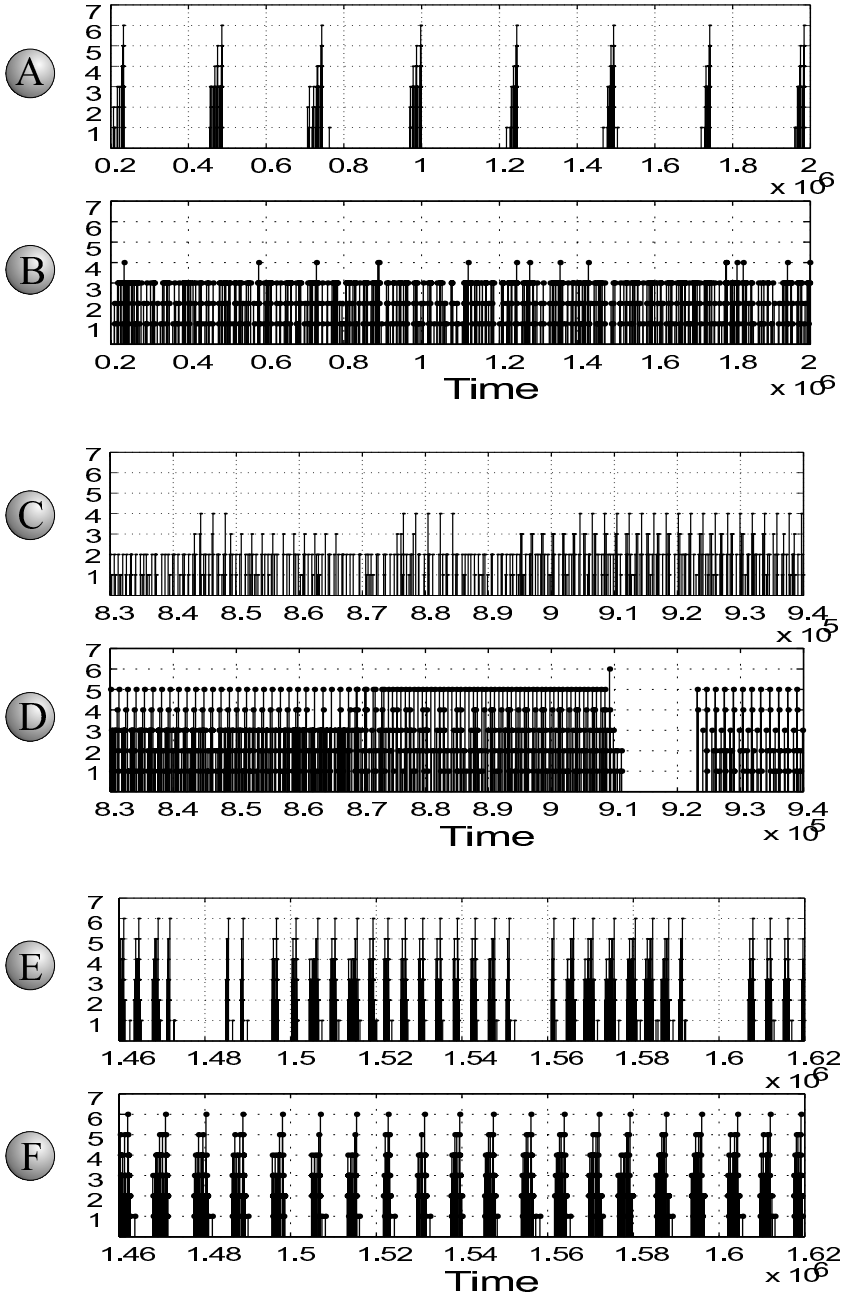

Figure 8: Synthetic sequences corresponding to the points along the trajectory in parameter space (Fig. 7a). The panels illustrate the transitions between the regimes **H** and **L** — panels (A) and (B); **L** and **I** — (C) and (D); and **I** and **H** — (E) and (F). The transition from (A) to (B) is very pronounced, while the other two transitions are smoother.